nature biotechnology

Brief Communication

https://doi.org/10.1038/s41587-023-01839-z

Detection of phosphorylation post-translational modifications along single peptides with nanopores

Received: 11 November 2022

Accepted: 23 May 2023

Published online: 29 June 2023

Check for updates

Ian C. Nova[1,3], Justas Ritmejeris[1,3], Henry Brinkerhoff[1,2,3], Theo J. R. Koenig[1], Jens H. Gundlach[2] & Cees Dekker[1]

Current methods to detect post-translational modifications of proteins, such as phosphate groups, cannot measure single molecules or differentiate between closely spaced phosphorylation sites. We detect post-translational modifications at the single-molecule level on immunopeptide sequences with cancer-associated phosphate variants by controllably drawing the peptide through the sensing region of a nanopore. We discriminate peptide sequences with one or two closely spaced phosphates with 95% accuracy for individual reads of single molecules.

Post-translational modifications (PTMs) play crucial roles in protein function and cell fate. Most PTMs involve attachment of a small chemical group (phosphoryl, acetyl, glycosyl and so on) to amino acids, which greatly expands the proteome. Mass spectrometry is the principal technique to detect PTMs, but this method requires substantial sample input (typically >10^9 copies) and often struggles to identify the correct position of a PTM between multiple candidate sites[1]. Improved detection of protein phosphorylation, the most frequent PTM[2], is of particular interest, as dysregulation of phosphorylation pathways is linked to many diseases including cancers, Parkinson's, Alzheimer's and heart disease[3]. Specifically, certain phosphorylation patterns on immunopeptides, which are naturally digested protein products on the cell surface for immune cell recognition, have been directly linked to cancer cells, making these immunopeptide variants promising neoantigens (cancer-specific antigens) for targeted immunotherapy or cancer screening[4]. Nanopore techniques, where the change in ion current is measured as a single molecule passes through a nanopore in a membrane, have shown promise for PTM detection[5–13]. However, these approaches, which measure brief transient blockades, have so far lacked high accuracy in variant identification for single molecules.

In this Brief Communication, we apply a recently introduced nanopore single-peptide scanning method[14–16] to PTM detection and demonstrate its capabilities to detect and discriminate single phosphate groups within individual peptides. In this approach[14], a peptide of interest (up to ~25 amino acids) is chemically linked to a DNA oligonucleotide, creating a peptide–oligonucleotide conjugate (POC) that is slowly translocated in a stepwise manner through a nanopore (MspA[17]) using a DNA motor enzyme (Hel308 helicase[18]), as in nanopore DNA sequencing[19–22]. Previously[14], individual amino acid substitutions on single peptides were discriminated with high accuracy, but the peptide sequence tested was atypical, with a near-uniform negatively charged chain of aspartate and glutamate residues to induce electrophoretic insertion of the POC into the nanopore. To test biologically relevant peptides with various charges, we chemically linked a second DNA oligo (the 'threading DNA') to the other end of the peptide[16] (Fig. 1a). This DNA electrophoretically threads the POC into and through the nanopore where it is subsequently pulled back out of the pore in ~0.3 nm steps by the helicase, slowly scanning the peptide across the narrow sensing constriction of the pore (Fig. 1b). Figure 1c depicts a typical ion current trace from a single translocation event of a POC containing a 10-amino-acid peptide. The first part of the trace reads the template DNA section that corresponds well with the predicted pattern from nanopore DNA sequencing[22] (Fig. 1d), whereas the second part contains the linker and peptide signal of interest.

We found that this approach allows extremely sensitive measurements that can clearly distinguish peptides with or without a single PTM. We measured POCs containing the immunopeptide BCAR3 (Fig. 1e), a promising neoantigen for immunotherapy[4]. We compared BCAR3 (with sequence LKEPTRDMI, written C to N terminus) and its phosphate-PTM-containing variant pBCAR3 where a single threonine

[1]Department of Bionanoscience, Kavli Institute of Nanoscience Delft, Delft University of Technology, Delft, the Netherlands. [2]Department of Physics, University of Washington, Seattle, WA, USA. [3]These authors contributed equally: Ian C. Nova, Justas Ritmejeris, Henry Brinkerhoff.
e-mail: c.dekker@tudelft.nl

https://doi.org/10.1038/s41587-023-01839-z

residue was phosphorylated (LKEP[pT]RDMI). Consensus ion current patterns were determined by aligning and averaging $n = 40$ reads of each variant (Fig. 1f). The addition of phosphothreonine (pT), a single small PTM of only five atoms, produced a dramatic change to the current pattern. Specifically, the pattern for the phosphate-containing variant was consistent with unphosphorylated BCAR3 until pT entered the sensing region, whereupon the current increased significantly by up to 25% for 13 steps, until the current returned to match for the rest of the remaining steps. These data clearly show that a single PTM can be well distinguished with even one nanopore read of a single molecule.

We next demonstrated the sensitivity of this method to discriminate between closely spaced PTMs along a peptide. We repeated the procedure to analyze another clinically relevant immunopeptide[4], βCAT (AGSHIGSDLY), that contains two phosphorylation sites, one at each serine (termed pS1 and pS2), at positions separated by three amino acids (Fig. 1e). We determined the current patterns for the unphosphorylated variant, both single-phosphoserine (pS) variants (p1βCAT containing pS1, AG[pS]HIGSDLY; and p2βcat containing pS2, AGSHIG[pS]DLY), and the double pS variant (p1p2βCAT containing both pS1 and pS2, AG[pS]HIG[pS]DLY) (Fig. 1g). All four βCAT variants produced a distinct ion current pattern that could clearly be discriminated from that of the other variants. Just like for pT (Fig. 1f), the addition of pS had the consistent effect of increasing the current. Notably, the magnitude of the increase and the number of steps that were affected varied between the two single phosphorylation sites (9 steps for p1βCAT and 12 steps for p2βCAT). For the double phosphopeptide (p1p2βCAT), the two phosphoserines combined to increase the current even more than with the two single variants, reaching large current values that exceeded the nonphosphorylated variant by up to 64% for 12 steps.

These differences in ion current patterns can be used to accurately identify the correct variant for individual reads of these immunopeptides—as can be quantified in a so-called confusion matrix. For 198 single reads of BCAR3 and its variant, we blindly determined the correct variant using a hidden Markov model with an accuracy of 93% (Fig. 1h). For 562 reads of βCAT and its variants, we determined the correct variant with 95% accuracy, while individual variant-calling accuracies ranged between 91% (βCAT) and 98% (p2βCAT) (Fig. 1i). Overall, the single-read variant-calling accuracy was 95% for all of the measured phosphopeptides, highlighting the capabilities of this technique to reliably determine the correct PTM location on single molecules.

The heterogeneous charge profile of these peptides leads to variations in the POC polymer's stretching as it is stepped through the pore. The constant *k*-mer reading frame[19] that is commonly used in models of nanopore DNA sequencing is therefore inadequate to describe the influence of amino acid sequence on ion current patterns. We developed a physical model to better understand this behavior. For each of the four βCAT variants, we performed a Markov-chain Monte Carlo (MCMC) calculation (Methods), where the POC was modeled as a freely jointed chain with units of varying charge (Fig. 2a), anchored at the top of the MspA pore by Hel308, and subject to ion-screened Coulomb forces between charges as well as to the applied electrostatic potential (Fig. 2b). By performing the MCMC calculation with each βCAT variant at 30 consecutive Hel308 steps, we simulated the movement of the POCs through the nanopore. Figure 2c depicts typical configurations found for p2βCAT at a selection of Hel308 steps, while Fig. 2d plots the corresponding mean *z*-location (vertical axis along the pore) of the pS2 PTM, calculated for every step. We find that, after the template DNA is stepped through the sensing region, the linker/peptide polymer bunches within the pore, until the large negative charge (pS2) is held just below the nanopore constriction by the voltage drop. As stepping continues, the slack is gradually pulled out of the polymer and the phosphate is slowly pulled up into the pore constriction, reaching a critical point at which the charged phosphate quickly pops up into the pore vestibule and the polymer returns to a bunched slack configuration. This is illustrated in the trace of Fig. 2d where the pS2 PTM stalls at $z \sim 8$ nm, until it suddenly jumps up at step 19. While residing in the stalling position just below the pore, the negative phosphate group probably promotes the transit of K^+ ions, thus increasing the nanopore current, as seen in the experimental data (Fig. 1g). The stalling and jumping behavior was consistently observed for all PTMs in all βCAT peptides (Fig. 2e).

As a proxy for the ion current patterns, we extracted the percentage of time that a phosphate PTM was present in the sensing region (defined as $6.6\ \text{nm} < z < 8.2\ \text{nm}$, Methods) at each step in the simulations (Fig. 2f). The results display an excellent correspondence with the experimental ion current differences (Fig. 2g), capturing the wider region of influence for pS2 in p2βCAT compared to pS1 in p1βCAT (12 steps versus 9 steps). In addition, the combined effect of pS1 and pS2 in p1p2βCAT influencing the same region as pS2 on its own in p2βCAT (12 total steps for both, Fig. 2g) is well represented by the model (Fig. 2f). Overall, this model provides a starting point for understanding how the charge distribution along peptides relates to ion current traces. In addition, this type of modeling provides a future pathway towards accurate PTM mapping, where the expected region of influence can be used to identify the amino acid location of a PTM along the peptide.

Our data provide demonstration of a technique that can accurately differentiate between single-molecule phosphopeptide variants by controllably drawing the peptide through the sensing region of a nanopore. The technique can clearly distinguish phosphopeptides with phosphates that are separated by only a few amino acids (three in our example), where mass spectrometry faces particular difficulties, and it does not require chemical labeling of the PTM as in other single-molecule proteomics methods[23]. Notably, nanopores were previously used to distinguish peptide variants with PTMs during free

Fig. 1 | Nanopore PTM detection experimental schematic and data workflow. **a**, Schematic of the POC. A (phosphorylated) immunopeptide (pink) is linked by its C-terminus to the 5′ end of a DNA template (linker 1, cysteine–maleimide bond), while its N-terminus is linked to the 5′ end of the threading DNA (linker 2, azide-DBCO bond). Hel308 helicase loads onto the single-stranded DNA/double-stranded DNA junction made by a complementary oligo (comp DNA) that is annealed to the template DNA. **b**, Schematic of POC reading. An MspA nanopore (gray) is embedded in a lipid bilayer. Applied voltage (180 mV) drives a current of K^+ and Cl^- ions through the nanopore. The threading DNA is electrophoretically driven into and through the nanopore, translocating the POC, stripping off the comp DNA and docking the Hel308 onto the rim of MspA. As Hel308 steps along the template DNA, the POC is pulled up through the pore in ~0.33 nm increments, thereby pulling residues through the narrowest portion of MspA (sensing region) where they modulate the ion current. **c**, Ion current trace of a typical POC reading event for βCAT. Ion currents (I) are normalized to the unblocked open-state pore current (I_{os}). Measured levels (red) are determined using a data segmentation algorithm. After reading the template DNA, linker 1 enters the sensing region (at 5 s), followed by peptide, linker 2, and the start of the threading DNA. **d**, Consensus sequence of ion current steps (red), which in the DNA section is closely matched by the ion current levels predicted by the DNA sequence (blue). Error bars in the measured ion current levels are errors in the mean value, often too small to see. Error bars in the prediction are standard deviations of the ion current levels that were used to build the predictive map[25]. **e**, Immunopeptides with amino acid sequences and phosphorylation sites. BCAR3 contains a single phosphorylation site at a threonine residue (pT). βCAT contains two serine phosphorylation sites (termed pS1 and pS2) separated by three amino acids. Phosphopeptide variants studied were BCAR3, pBCAR3 (with pT), βCAT, p1βCAT (with pS1), p2βCAT (with pS2) and p1p2βCAT (with both pS1 and pS2). **f**, Consensus ion current patterns for BCAR3 and for the PTM variant pBCAR3 (data are the mean value with standard deviation for $N = 40$ reads for each trace). Dashed line marks the end of the template DNA in the sensing region. **g**, Consensus ion current patterns for βCAT and its phosphopeptide variants (data are the mean value with standard deviation for $N = 40$ reads for each trace). **h**, Single-read blinded-variant-calling matrix for BCAR3 variants yielding an overall variant-calling accuracy of 93%. **i**, Same for βCAT variants, yielding an overall variant-calling accuracy of 95%.

https://doi.org/10.1038/s41587-023-01839-z

translocation[5], but the method developed presently, which analyzes the changes in current patterns over many subsequent steps (Fig. 1), presents a greatly improved sensitivity and versatility, and is capable of detection of both PTMs and amino acid substitutions[14].

While the accuracy that we realized was already very high (95%) in single reads, it can, if desired, be further improved upon using the rereading capability[14] of our nanopore scanning approach, as is illustrated in Supplementary Figs. 11–13 and described in detail in

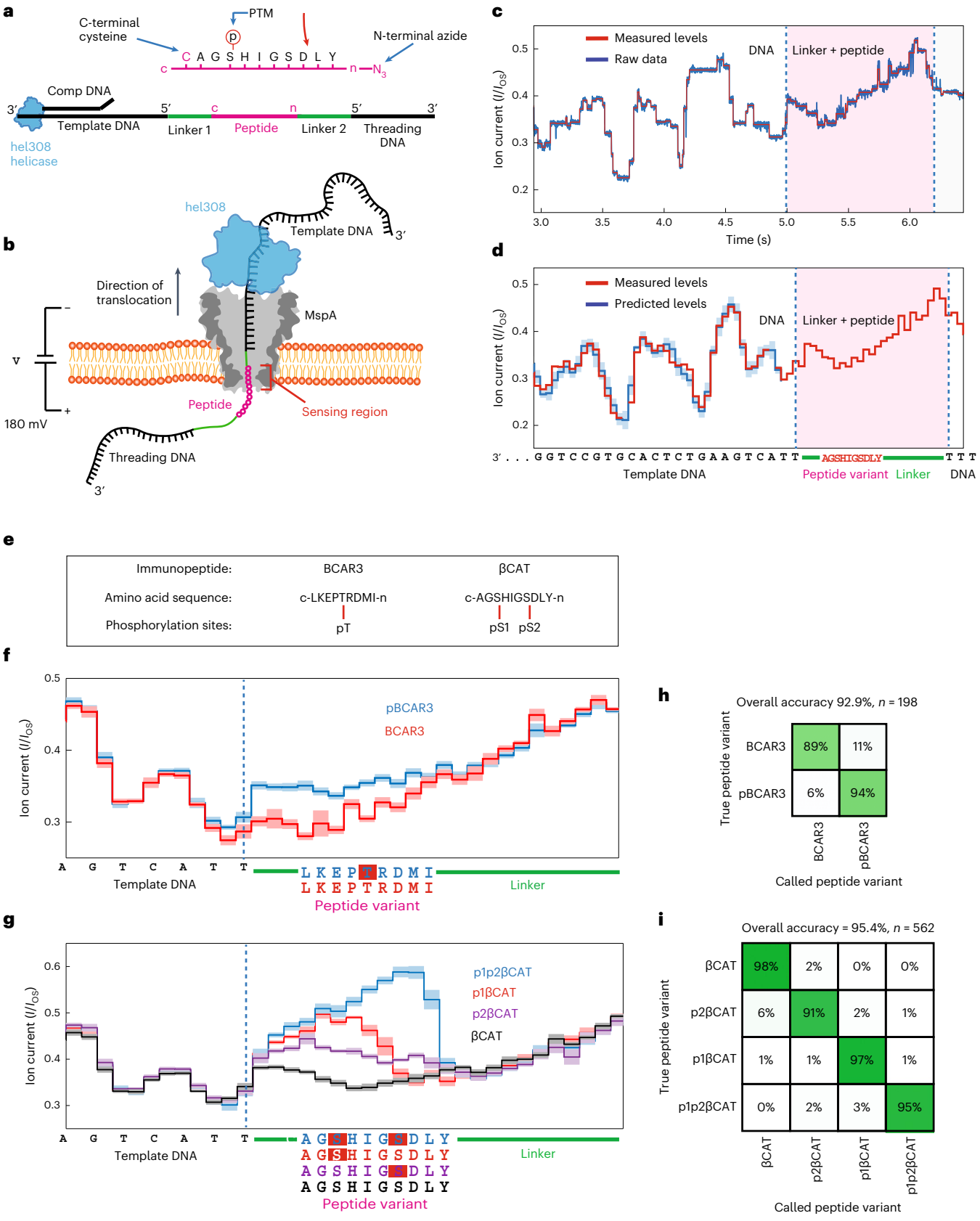

https://doi.org/10.1038/s41587-023-01839-z

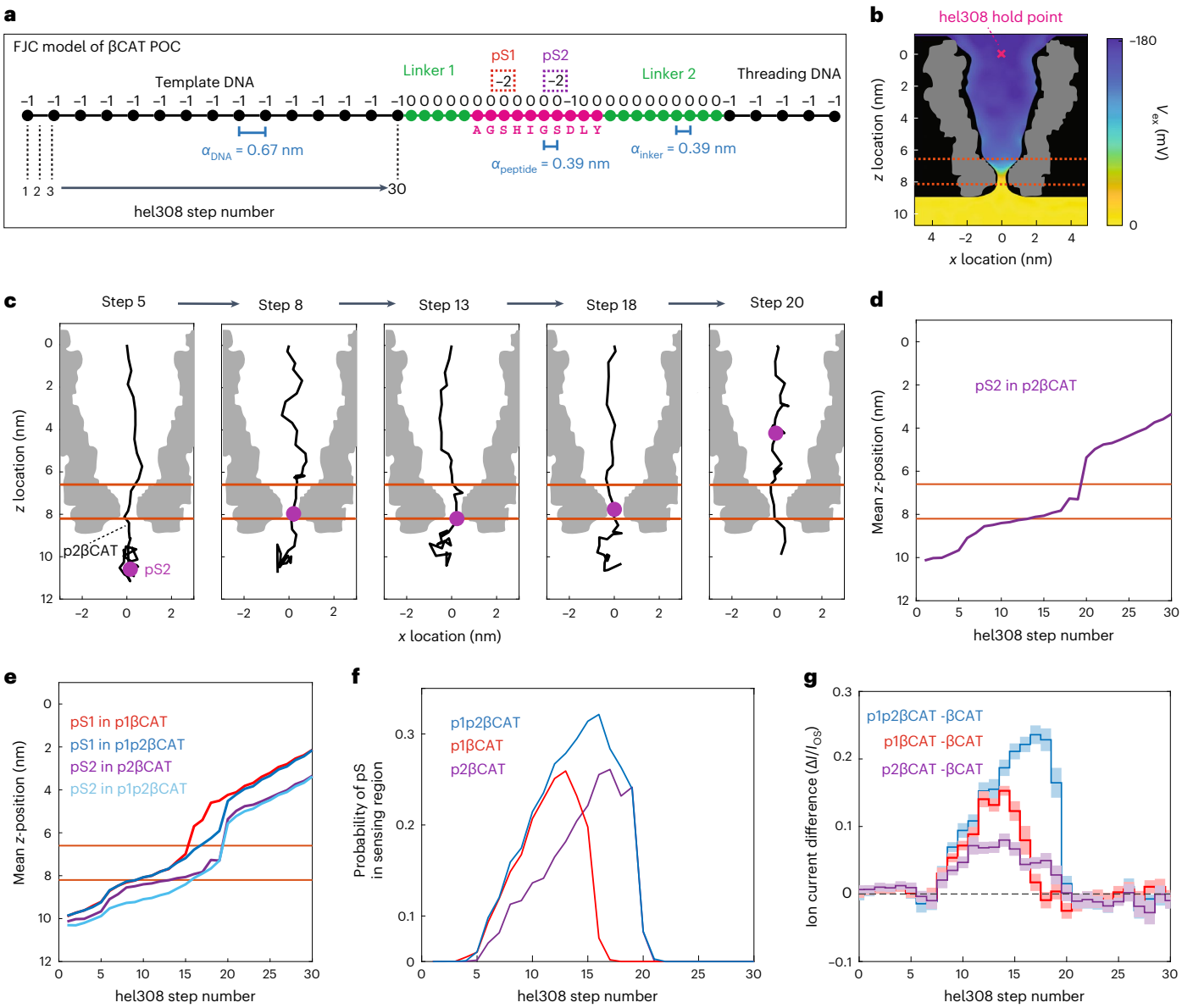

Fig. 2 | MCMC calculations of phosphate-containing peptides. a, Freely jointed chain (FJC) model of a POC-containing peptide βCAT. Each unit in the polymer has an electrical charge and a typical distance α between residues. Phosphoserine PTMs pS1 and pS2 add a charge of −2 to that unit. **b**, Electric potential profile (color gradient) in the MspA pore[26]. The POC was confined within the physical boundaries of MspA (black) and anchored at the Hel308 hold point (pink x). The volumetric map of the MspA cross-section is shown in gray. **c**, Snapshots of the polymer configuration within MspA from MCMC calculations for the p2βCAT POC at five Hel308 steps. The phosphoserine residue (pS2) (purple) is observed to move through the pore in a nonlinear fashion. Note that the POC polymer gets stretched towards Hel308 step 19, after which the PTM moves into the pore lumen and the polymer relaxes. Orange lines indicate the sensing region of MspA. **d**, Mean *z*-location of the pS2 PTM versus Hel308 step number. **e**, Same for all PTMs in the peptide variants. **f**, Probability that a pS occupied the sensing region for various βCAT PTM variants versus Hel308 step. **g**, Experimentally measured ion currents for βCAT phosphopeptide variants where the ion current measured for the non-PTM βCAT was subtracted (from data in Fig. 1g). Shaded error bar is the standard deviation.

Supplementary Text 2. This analysis revealed a residual variant-calling error due a finite synthesis purity of our test samples. The difficulty in assessing low error rates such as these (comparable to the percent impurity of the sample) also underscores the need for high-quality peptide and PTM standards as single-molecule peptide analysis tools become more accurate.

Detection of other PTM types (acetylation, hydroxylation, methylation and so on) can probably be achieved with an identical approach, as long as the PTM is not too bulky to translocate through MspA. It is of interest to note that the charge profile of the peptide sequences tested here was heterogeneous, and mixed-charge peptides did not impede the generation of well-reproducible current traces upon scanning these peptides through the pore. In addition to the anionic sequences tested in our previous work[14], this demonstrates the versatility of this method for PTM or amino acid composition analysis on a wide variety of peptide sequences and charges. Highly cationic peptides are thus far untested and may pose additional challenges, but such sequences are rare within the proteome[24].

Further method developments may involve increasing throughput using arrays of nanopores in parallel, developing robust methods to attach DNA to the N- and C-termini of peptides without the a priori modifications used here, and using this to move from using synthetic peptides to natural peptides collected from a biological sample. Engineering improvements could also be implemented to reduce the

read-head size and stretch the peptide, using nanopore protein engineering to increase the pore height and minimize the sensing region, or adding charged residues to increase the electroosmotic forces within the pore[25]. Even before such next steps, this demonstration of single PTM detection within individual peptides presents a tool for phosphorylation investigation, enabling measurements currently unachievable with other proteomics tools.

Online content

Any methods, additional references, Nature Portfolio reporting summaries, source data, extended data, supplementary information, acknowledgements, peer review information; details of author contributions and competing interests; and statements of data and code availability are available at https://doi.org/10.1038/s41587-023-01839-z.

References

1. Kim, M. S., Zhong, J. & Pandey, A. Common errors in mass spectrometry-based analysis of post-translational modifications. *Proteomics* **16**, 700–714 (2016).
2. Khoury, G. A., Baliban, R. C. & Floudas, C. A. Proteome-wide post-translational modification statistics: frequency analysis and curation of the swiss-prot database. *Sci. Rep.* **1**, 1–5 (2011).
3. Xu, H. et al. 'PTMD: a database of human disease-associated post-translational modifications'. *Genomics Proteomics Bioinformatics* **16**, 244–251 (2018).
4. Engelhard, V. H. et al. MHC-restricted phosphopeptide antigens: preclinical validation and first-in-humans clinical trial in participants with high-risk melanoma. *J. Immunother. Cancer* **8**, e000262 (2020).
5. Rosen, C. B. et al. Single-molecule site-specific detection of protein phosphorylation with a nanopore. *Nat. Biotechnol.* **32**, 179–181 (2014).
6. Restrepo-Pérez, L., Wong, C. H., Maglia, G., Dekker, C. & Joo, C. Label-free detection of post-translational modifications with a nanopore. *Nano Lett.* **19**, 7957–7964 (2019).
7. Huo, M. Z., Hu, Z. L., Ying, Y. L. & Long, Y. T. Enhanced identification of tau acetylation and phosphorylation with an engineered aerolysin nanopore. *Proteomics* **22**, 2100041 (2022).
8. Li, S. et al. T232K/K238Q aerolysin nanopore for mapping adjacent phosphorylation sites of a single tau peptide. *Small Methods* **4**, 2000014 (2020).
9. Wloka, C. et al. Label-free and real-time detection of protein ubiquitination with a biological nanopore. *ACS Nano* **11**, 4387–4394 (2017).
10. Shorkey, S. A., Du, J., Pham, R., Strieter, E. R. & Chen, M. Real-time and label-free measurement of deubiquitinase activity with a MspA nanopore. *ChemBioChem* **22**, 2688–2692 (2021).
11. Nir, I., Huttner, D. & Meller, A. Direct sensing and discrimination among ubiquitin and ubiquitin chains using solid-state nanopores. *Biophys. J.* **108**, 2340–2349 (2015).
12. Fahie, M. A. & Chen, M. Electrostatic interactions between OmpG nanopore and analyte protein surface can distinguish between glycosylated isoforms. *J. Phys. Chem. B* **119**, 10198–10206 (2015).
13. Versloot, R. C. A. et al. Quantification of protein glycosylation using nanopores. *Nano Lett.* **22**, 5357–5364 (2022).
14. Brinkerhoff, H., Kang, A. S., Liu, J., Aksimentiev, A. & Dekker, C. Multiple rereads of single proteins at single–amino acid resolution using nanopores. *Science* **374**, 1509–1513 (2021).
15. Yan, S. et al. Single molecule ratcheting motion of peptides in a *Mycobacterium smegmatis* porin A (MspA) nanopore. *Nano Lett.* **21**, 6703–6710 (2021).
16. Chen, Z. et al. Controlled movement of ssDNA conjugated peptide through *Mycobacterium smegmatis* porin A (MspA) nanopore by a helicase motor for peptide sequencing application. *Chem. Sci.* **12**, 15750–15756 (2021).
17. Butler, T. Z., Pavlenok, M., Derrington, I. M., Niederweis, M. & Gundlach, J. H. Single-molecule DNA detection with an engineered MspA protein nanopore. *Proc. Natl Acad. Sci. USA* **105**, 20647–20652 (2008).
18. Derrington, I. M. et al. Subangstrom single-molecule measurements of motor proteins using a nanopore. *Nat. Biotechnol.* **33**, 1073–1075 (2015).
19. Manrao, E. A. et al. Reading DNA at single-nucleotide resolution with a mutant MspA nanopore and phi29 DNA polymerase. *Nat. Biotechnol.* **30**, 349–353 (2012).
20. Cherf, G. M. et al. Automated forward and reverse ratcheting of DNA in a nanopore at 5-Å precision. *Nat. Biotechnol.* **30**, 344–348 (2012).
21. Laszlo, A. H. et al. Detection and mapping of 5-methylcytosine and 5-hydroxymethylcytosine with nanopore MspA. *Proc. Natl Acad. Sci. USA* **110**, 18904–18909 (2013).
22. Laszlo, A. H. et al. Decoding long nanopore sequencing reads of natural DNA. *Nat. Biotechnol.* **32**, 829–833 (2014).
23. Swaminathan, J. et al. Highly parallel single-molecule identification of proteins in zeptomole-scale mixtures. *Nat. Biotechnol.* **36**, 1076–1082 (2018).
24. Requião, R. D. et al. Protein charge distribution in proteomes and its impact on translation. *PLoS Comput. Biol.* **13**, e1005549 (2017).
25. Huang, G. et al. Electro-osmotic capture and ionic discrimination of peptide and protein biomarkers with FraC nanopores. *Nat. Commun.* **8**, 935 (2017).
26. Metropolis, N., Rosenbluth, A. W., Rosenbluth, M. N., Teller, A. H. & Teller, E. Equation of state calculations by fast computing machines. *J. Chem. Phys.* **21**, 1087–1092 (1953).

https://doi.org/10.1038/s41587-023-01839-z

Methods

Construction of POCs

Peptides (sequences in Supplementary Table 1) were purchased from Life Technologies and diluted to 10 µM in degassed PBS buffer. Phosphorylated amino acids were incorporated during solid-phase peptide synthesis. DNA oligos (sequences in Supplementary Table 2) were purchased from Biomers and diluted to 100 µM in degassed PBS buffer. Orthogonal click-chemistry reactions were used to attach a C-terminal cysteine on the peptide to a 5′ maleimide on the template DNA, and to attach a N-terminal azide on the peptide to a 5′ dibenzocyclooctyne group (DBCO) on the threading DNA.

The cysteine–maleimide reaction and the DBCO-azide copper-free click reaction were performed in one pot. Peptides and DNAs were mixed at a ratio of 1:2:6 (peptide:threading DNA:template DNA) at a concentration of 7 µM peptide in PBS and were incubated for 20 h at +4 °C under argon gas (50 µl reaction volume). Excess DNA was used to ensure the majority of peptide was conjugated. Supplementary Fig. 1 depicts the chemical structure of the full POC. The mixture was purified using DynaBeads strep-biotin polyA cleanup, ensuring that only constructs containing threading DNA (poly T) remained. The resulting product was estimated to be at a final concentration of 12.5 µM (20 µl elution volume) based on the maximum binding capacity of the beads. Comp DNA was added at a concentration of 15 µM and annealed to template DNA. The construction of the entire POC was verified using the nanopore measurements. Approximately 90% of the reads measured contained the entire POC construct. The other ~10% contained only template DNA, indicating that some template DNA without peptide remained after purification.

Nanopore experimental methods

Nanopore measurements were conducted as in Brinkerhoff et al.[14] and previous studies[17–22] with a few notable differences. DPhPC lipids purchased from Avanti were used to paint bilayers on ~10 µM Teflon apertures in custom U-tube experimental devices. MspA mutant M2-NNN[17] was purified by Genscript. All experiments were conducted at 37 ± 1 °C with 1 mM ATP, 400 mM KCl, 10 mM $MgCl_2$, 10 mM HEPES pH 8.00 ± 0.05 in the *cis* well and 400 mM KCl, 10 mM HEPES pH 8.00 ± 0.05 in the *trans* well. Hel308 was added to the *cis* well to a final concentration of 50 nM. POCs were added to a final concentration of 5 nM. Hel308 used in this study is from *Thermococcus gammatolerans* (accession number WP_015858487.1) and was cloned into the pET-28b(+) vector plasmid at NdeI/NotI sites by Genscript. Ion current data were acquired at 50 kHz sampling frequency using an Axopatch 200B patch clamp amplifier and filtered with 10 kHz 4-pole Bessel filter. Applied voltage was set to 180 mV for all experiments and controlled by a National Instruments X series DAQ and operated with custom LabVIEW software. Using these methods, many ion current reads (termed 'events') were gathered for each of the six POCs used in this study.

Data analysis

All data analysis was performed in MATLAB. Custom MATLAB software as described in detail in Brinkerhoff et al.[14], and briefly below, was used for data preprocessing, reduction, filtering, alignment and variant identification:

Event selection and filtering. Data were further Bessel filtered and decimated to 5 kHz, and potential events were identified using a thresholding algorithm based on the unblocked pore current as in previous work[14,17–22]. Events were then selected by eye by discrete selection criteria for further analysis. Occasionally, Hel308 fell off of the DNA before the end of the template strand. Therefore, we selected events that included steps for both template DNA and the entire peptide region into the second linker (for example events that fit selection criteria, see Supplementary Figs. 2–7).

Level finding and filtering. To determine the transition points between Hel308 steps in the data, we used a change point algorithm as described in previous work[17] and originally developed in Wiggins et al.[27]. A sample of the typical behavior of this change point 'level finder' across an entire event is shown in Supplementary Fig. 8. These measured levels were further filtered, first by excluding any levels outside the bounds of expected current values ($I/I_{OS} < 0.15$ or $I/I_{OS} > 0.7$). Levels outside of these bounds correspond to noise spikes or mid-event gating of MspA pore. We next applied a recombination filter, as described in Noakes et al.[28], which identifies helicase backsteps and eliminates repeated levels from the trace. We delineated each event by eye by noting the position of the end of the DNA template in the measured levels, creating a DNA section (before this position) and peptide section (after this position, including both linker 1 and peptide and linker 2) for each event.

Reread removal. In our previous study[14], it was determined that, at high Hel308 concentration, a string of multiple Hel308 enzymes can be loaded onto the DNA template strand during translocation. After the first Hel308 reaches the end of the DNA template and dissociates, the POC falls back through the pore until the next Hel308 sits on the rim of the pore and continues stepping. This produces a 'reread' of the polymer, where the reread usually includes the final ~16 steps (equal to the footprint of one Hel 308 enzyme, 8 DNA bases). In the experiments presented in the main text, the rereads did not include the variable region within the peptide but merely included levels corresponding to linker 2 within the pore (Supplementary Figs. 9 and 10). However, rereading of the relevant region was enabled by using a different linker design (Supplementary Text 1). In the current study, rereads were removed for subsequent analysis. Supplementary Fig. 9 depicts a typical rereading pattern and sections of removal.

DNA level prediction. The current pattern for the template DNA sequence was predicted using an empirically derived 6-mer map[29], where each six-base sequence was given two ion current states, corresponding to the two substeps of Hel308 helicase ('pre' and 'post' steps) per DNA base. The ion currents in the map are the mean of the set of ion currents assigned to each state, and the uncertainty in the ion current is the standard deviation in that set of ion currents. The prediction matched well with the experimentally measured DNA levels in this study (Fig. 1d).

Initial consensus generation. For the peptide section of the measured ion current, the ion current patterns had to be experimentally determined for each POC variant, as no predictive map exists for peptides or other polymers that are not DNA or RNA. To determine the ion current patterns for the linker and peptide regions of each POC (Fig. 1), we determined an initial 'best guess' of the ion current pattern. A selection of typical reads ($n = 6–10$) of each construct was compared by eye to determine the unique ion current states and place them in the appropriate order. This process eliminated Hel308 backsteps, repeated levels and spurious states that are not representative of typical reads. These initial consensuses included the last 15 steps of the DNA template section and 28 steps after the DNA template (where the helicase typically fell off of the DNA).

Reads were then calibrated, applying a scaling factor m to the measured ion current to account for slight variations in buffer salt concentration due to evaporation. Determination of the scaling factor was done as in Brinkerhoff et al.[14], where the maximum likelihood estimator for m that limited the error between reads was calculated for each read. After applying the scales, a mean and standard deviation value was calculated for each position in the consensus. Next, a second round of calibration was applied to the mean consensus values in order to ensure cross-calibration consistency between consensus of the different POC variants. We calculated a scale and offset factor by performing a single-polynomial fit of the first 15 steps of each initial consensus (corresponding to the DNA section) to the last 15 levels of the predicted ion current pattern for the DNA template sequence.

This ensured that all of the consensus patterns were calibrated to the same reference.

Final consensus generation. These calibrated initial consensuses were then used as initial guesses for a customized Baum–Welch algorithm, a type of expectation maximization for the hidden Markov model. This algorithm was performed identically as in Brinkerhoff et al.[14] and described fully in Noakes et al.[28]. We randomly chose 40 events of each POC variant for the EM algorithm. To calibrate these events, we performed a hidden-Markov-model alignment of the levels in the DNA section of each event to the template DNA prediction over a range of scale factors (m = 0.8 to 1.2 with increments of 0.01) and calculated a likelihood score for each m value. We chose the m value that produced the highest alignment score. We then applied this event specific scale factor to the associated measured levels from the peptide section of the same event. The expectation maximization algorithm was then used to generate a final consensus for each POC variant, using this set of calibrated events of each variant and the initial consensus as a seed for the algorithm. Using this procedure, we obtained six final consensus ion current patterns (one for each of the immunopeptide variants used in this study). Figure 1f,g depicts the final consensus ion current patterns for each immunopeptide variant.

Variant identification. All filtered events that were not included in the initial or final consensus were used for variant identification. We calibrated each set of peptide levels using the DNA section alignment as previously. For each set of now calibrated peptide section levels, we performed a hidden Markov model alignment to the final consensus for each variant. Events containing βCAT and its associated variants were separated from BCAR3 and its associated variant and only aligned to the set of variants of the appropriate immunopeptide. The alignment producing the maximum alignment score was chosen as 'called variant' (Fig. 1h,i). Alignment accuracy for each variant was calculated as the percentage of correct calls compared to the total number of calls. The overall accuracy was calculated by calculating the percentage of correct calls for all variants divided by total calls.

Simulation methods

MCMC calculations[26] were implemented in MATLAB. Degrees of freedom were encoded as polar and azimuthal angles between each polymer joint, with the first joint being fixed at the origin located at the top of MspA's vestibule. Spacings between joints were chosen to be 0.67 nm for DNA and 0.39 nm for linker and peptide regions. Charges were assigned to each joint: $+1e^-$ for each K or R residue, $-1e^-$ for each D or E residue and for each DNA monomer, $-2e^-$ for each phosphorylated residue, and 0 for all other joints (Supplementary Fig. 14). The update distribution for both the polar and azimuthal angles was a normal distribution with mean 0 and standard deviation 0.05 radians.

The potential energy was calculated as the sum of (1) the interaction between the joint charges and a previously published electric potential map of MspA (Supplementary Fig. 15)[30]; (2) the Coulomb interaction between pairs of joint charges, screened with a Debye radius of 0.40 nm; and (3) a hard wall excluding any polymer joints from the wall of MspA, defined using a cylindrically symmetric spline derived from the electric potential map.

The MCMC calculation was performed at different 'enzyme steps' by removing monomers from the top part of the chain one by one, thereby shifting the entire sequence up through the constriction. At each step, the calculation started with a completely extended chain, with all polar and azimuthal angles set to 0, and the calculation was iterated 10^6 times. We discarded the first 10^4 samples at each step in order to allow for thermalization of the samples before inclusion in the calculated distributions (for a detailed description of the simulations, see Supplementary Text 2).

Figure 2f was produced by computing the fraction of samples in which a phosphorylation lay in the region where the z-component of the electric field along the z axis was greater than $1\,k_BTe^{-1}\,nm^{-1}$ per electron (6.6 nm < z < 8.2 nm, Supplementary Fig. 16) Figure 2d,e was produced by computing the mean position of the phosphorylated residue in the samples for each construct during each step.

Reporting summary

Further information on research design is available in the Nature Portfolio Reporting Summary linked to this article.

Data availability

The raw nanopore data for all of the reads used in this study are publicly available at https://doi.org/10.57760/sciencedb.08338[31].

References

27. Wiggins, P. A. An information-based approach to change-point analysis with applications to biophysics and cell biology. *Biophys. J.* **109**, 346–354 (2015).
28. Craig, J. M. et al. Determining the effects of DNA sequence on Hel308 helicase translocation along single-stranded DNA using nanopore tweezers. *Nucleic Acids Res.* **47**, 2506–2513 (2019).
29. Noakes, M. T. et al. Increasing the accuracy of nanopore DNA sequencing using a time-varying cross membrane voltage. *Nat. Biotechnol.* **37**, 651–656 (2019).
30. Bhattacharya, S., Yoo, J. & Aksimentiev, A. Water mediates recognition of DNA sequence via ionic current blockade in a biological nanopore. *ACS Nano* **10**, 4644–4651 (2016).
31. Nova, I. C. Nanopore data traces for PTM detection on peptides. *Science Data Bank* https://doi.org/10.57760/sciencedb.08338 (2023).

Acknowledgements

We thank A. Laszlo for discussions on the MCMC calculations, J. van der Torre for help in troubleshooting POC construction, E. van der Sluis and A. Goutou for Hel308 purification, and A. Aksimentiev for discussions. The work was supported by funding from the Dutch Research Council (NWO) project NWO-I680 (SMPS) (C.D.); European Research Council Advanced Grant 883684 (C.D.); European Commission Marie Skłodowska-Curie Fellowship 897672 (H.B.); and NIH NHGRI project HG012544-01 (J.G. and C.D.).

Author contributions

H.B. and C.D. conceived of and designed the study. I.C.N., J.R. and T.J.R.K. performed nanopore experiments. J.R. established and troubleshooted the method for POC construction. I.C.N. performed computational analyses of the experimental data. H.B. performed the simulations. C.D. and J.H.G. supervised the work. I.C.N. wrote the initial manuscript draft, and all authors contributed to the writing of the final manuscript.

Competing interests

H.B. and C.D. have filed a provisional patent for the nanopore peptide measurement method (NL patent N2024579 P1600131NL00). The remaining authors declare no competing interests.

Additional information

Supplementary information The online version contains supplementary material available at https://doi.org/10.1038/s41587-023-01839-z.

Correspondence and requests for materials should be addressed to Cees Dekker.

Peer review information *Nature Biotechnology* thanks Meni Wanunu and the other, anonymous, reviewer(s) for their contribution to the peer review of this work.

nature portfolio

Corresponding author(s): Cees Dekker

Last updated by author(s): May 18, 2023

Reporting Summary

Nature Portfolio wishes to improve the reproducibility of the work that we publish. This form provides structure for consistency and transparency in reporting. For further information on Nature Portfolio policies, see our Editorial Policies and the Editorial Policy Checklist.

Statistics

For all statistical analyses, confirm that the following items are present in the figure legend, table legend, main text, or Methods section.

n/a	Confirmed	
☐	☒	The exact sample size (*n*) for each experimental group/condition, given as a discrete number and unit of measurement
☐	☒	A statement on whether measurements were taken from distinct samples or whether the same sample was measured repeatedly
☐	☒	The statistical test(s) used AND whether they are one- or two-sided *Only common tests should be described solely by name; describe more complex techniques in the Methods section.*
☐	☒	A description of all covariates tested
☐	☒	A description of any assumptions or corrections, such as tests of normality and adjustment for multiple comparisons
☐	☒	A full description of the statistical parameters including central tendency (e.g. means) or other basic estimates (e.g. regression coefficient) AND variation (e.g. standard deviation) or associated estimates of uncertainty (e.g. confidence intervals)
☒	☐	For null hypothesis testing, the test statistic (e.g. *F*, *t*, *r*) with confidence intervals, effect sizes, degrees of freedom and *P* value noted *Give P values as exact values whenever suitable.*
☐	☒	For Bayesian analysis, information on the choice of priors and Markov chain Monte Carlo settings
☒	☐	For hierarchical and complex designs, identification of the appropriate level for tests and full reporting of outcomes
☒	☐	Estimates of effect sizes (e.g. Cohen's *d*, Pearson's *r*), indicating how they were calculated

Our web collection on statistics for biologists contains articles on many of the points above.

Software and code

Policy information about availability of computer code

Data collection	Data was collected using 2018 LabVIEW software with custom
Data analysis	Data analysis was performed in Matlab R2022b. All Matlab software was developed in-house, including the data preprocessor, the level segmentation algorithm, the Baum-Welch algorithm, the HMM solving algorithm, and the Markov Chain Monte Carlo calculator.

For manuscripts utilizing custom algorithms or software that are central to the research but not yet described in published literature, software must be made available to editors and reviewers. We strongly encourage code deposition in a community repository (e.g. GitHub). See the Nature Portfolio guidelines for submitting code & software for further information.

Data

Policy information about availability of data

All manuscripts must include a data availability statement. This statement should provide the following information, where applicable:

- Accession codes, unique identifiers, or web links for publicly available datasets
- A description of any restrictions on data availability
- For clinical datasets or third party data, please ensure that the statement adheres to our policy

All of the data used in this study has been made publicly available for download https://doi.org/10.57760/sciencedb.08338.

Human research participants

Policy information about studies involving human research participants and Sex and Gender in Research.

Reporting on sex and gender	n/a
Population characteristics	n/a
Recruitment	n/a
Ethics oversight	n/a

Note that full information on the approval of the study protocol must also be provided in the manuscript.

Field-specific reporting

Please select the one below that is the best fit for your research. If you are not sure, read the appropriate sections before making your selection.

☒ Life sciences ☐ Behavioural & social sciences ☐ Ecological, evolutionary & environmental sciences

For a reference copy of the document with all sections, see nature.com/documents/nr-reporting-summary-flat.pdf

Life sciences study design

All studies must disclose on these points even when the disclosure is negative.

Sample size	Sample sizes of 75 reads were chosen for nanopore experiments to ensure uncertainties in identification accuracy percentages of less than ±5%, given initial estimates of accuracy. Sample sizes of 10^6 frames were generated for Monte Carlo calculations in order to reduce the noise in the constriction occupancy probability such that the curves in figure 3(f) were easily visually distinguishable.
Data exclusions	Data was excluded that did not fit the criteria for an event as outlined in the mthods section of the main text of the publication. This included events that did not contain the entire DNA or peptide section.
Replication	All data sets were acquired across 3 or more pores for each variant on different days. Data sets were consistent across pores, and data from all sets was included in the final accuracy calculations.
Randomization	The division of data into training sets and evaluation sets was performed by selecting a random subset of the unexcluded reads. Because this work was not a treatment/response study, further randomization of experimental groups was not relevant.
Blinding	All experimental steps were identical between each variant, with no opportunity for an investigator to affect the quality of the reads at these stages. Read identification was performed by fully blinded software supplied only with the sequence of ion current levels to make an identification.

Reporting for specific materials, systems and methods

We require information from authors about some types of materials, experimental systems and methods used in many studies. Here, indicate whether each material, system or method listed is relevant to your study. If you are not sure if a list item applies to your research, read the appropriate section before selecting a response.

Materials & experimental systems

n/a	Involved in the study
☒	☐ Antibodies
☒	☐ Eukaryotic cell lines
☒	☐ Palaeontology and archaeology
☒	☐ Animals and other organisms
☒	☐ Clinical data
☒	☐ Dual use research of concern

Methods

n/a	Involved in the study
☒	☐ ChIP-seq
☒	☐ Flow cytometry
☒	☐ MRI-based neuroimaging